Amyotrophic lateral sclerosis-linked mutations increase the viscosity of liquid-like TDP-43 RNP granules in neurons

Pallavi P. Gopal[a,b], Jeffrey J. Nirschl[b,c], Eva Klinman[b,c], and Erika L. F. Holzbaur[b,c,1]

[a]Department of Pathology and Laboratory Medicine, Perelman School of Medicine, University of Pennsylvania, Philadelphia, PA 19104; [b]Department of Physiology, Perelman School of Medicine, University of Pennsylvania, Philadelphia, PA 19104; and [c]Neuroscience Graduate Group, Perelman School of Medicine, University of Pennsylvania, Philadelphia, PA 19104

Edited by Don W. Cleveland, University of California, San Diego, La Jolla, CA, and approved February 3, 2017 (received for review August 29, 2016)

Ribonucleoprotein (RNP) granules are enriched in specific RNAs and RNA-binding proteins (RBPs) and mediate critical cellular processes. Purified RBPs form liquid droplets in vitro through liquid–liquid phase separation and liquid-like non–membrane-bound structures in cells. Mutations in the human RBPs TAR-DNA binding protein 43 (TDP-43) and RNA-binding protein FUS cause amyotrophic lateral sclerosis (ALS), but the biophysical properties of these proteins have not yet been studied in neurons. Here, we show that TDP-43 RNP granules in axons of rodent primary cortical neurons display liquid-like properties, including fusion with rapid relaxation to circular shape, shear stress-induced deformation, and rapid fluorescence recovery after photobleaching. RNP granules formed from wild-type TDP-43 show distinct biophysical properties depending on axonal location, suggesting maturation to a more stabilized structure is dependent on subcellular context, including local density and aging. Superresolution microscopy demonstrates that the stabilized population of TDP-43 RNP granules in the proximal axon is less circular and shows spiculated edges, whereas more distal granules are both more spherical and more dynamic. RNP granules formed by ALS-linked mutant TDP-43 are more viscous and exhibit disrupted transport dynamics. We propose these altered properties may confer toxic gain of function and reflect differential propensity for pathological transformation.

TDP-43 | ribonucleoprotein granules | liquid droplets | amyotrophic lateral sclerosis | neurons

Cellular organelles allow eukaryotic cells to organize biochemical processes and concentrate specific cellular reactions in space and time. Although the role of membrane-bound organelles in cytoplasmic compartmentalization has long been recognized, the distinct biophysical properties and functions of non–membrane-bound organelles enriched in RNA and proteins have been recognized only recently (1–5). Ribonucleoprotein (RNP) granules, such as P granules in *Caenorhabditis elegans* (1), nucleoli in *Xenopus laevis* oocytes (2), yeast P bodies (3), and mammalian stress granules (6), show liquid droplet properties (reviewed in refs. 5, 7, 8), including fusion with rapid relaxation to a spherical shape, dynamic internal rearrangements, and rapid dissolution and assembly. Proteins comprising RNP granules share a common structure containing both RNA recognition motifs (RRMs) and low-complexity sequences (LCSs), intrinsically disordered regions that mediate protein–protein interactions (7, 9). In vitro characterization of human RNP granule proteins, RNA-binding protein FUS and heterogeneous nuclear ribonucleoprotein A1 (hnRNP A1), which are mutated in rare inherited forms of amyotrophic lateral sclerosis (ALS) and frontotemporal dementia (FTD) (10–12), has revealed the LCS drives self-assembly of RNP granules through a process termed liquid–liquid phase separation (LLPS) (6, 13–18).

Among eukaryotic cells, neurons face unique challenges in spatiotemporal cytoplasmic organization related to their complex axonal-dendritic morphology, separation of soma and axon terminal, and long cellular lifetimes with limited capacity for regeneration. Functionally, neurons maintain distinct axonal and dendritic pools of mRNAs allowing for rapid responses to local environmental cues (19). RNA transport granules are specialized RNP organelles composed of RNA-binding proteins (RBPs), translationally repressed mRNA, and molecular motors that play a key role in establishing mRNA polarity (20, 21). However, it is unclear whether neuronal cytoplasmic RNP granules also display liquid droplet properties, and if so, how these biophysical properties underlie physiological functions and relate to disease.

TAR-DNA binding protein 43 (TDP-43), a highly conserved DNA-binding protein and RBP with two RRMs and a glycine-rich C-terminal LCS, is a component of RNA transport granules and cotransports with mRNA (22–26). Mutations in *TARDBP*, the gene encoding TDP-43, have been linked to familial and rare sporadic cases of ALS (27, 28). Moreover, neuronal and glial cytoplasmic inclusions composed of TDP-43 serve as the neuropathological hallmark of sporadic ALS and the majority of FTD cases (29). In vitro characterization of TDP-43 has been limited by its tendency to fibrillize (15, 30). Although a recent study in mammalian cells demonstrates that nuclear TDP-43 may also undergo LLPS to form multiphase compartments (31), the biophysical properties of TDP-43 RNP granules have not been examined in neurons.

We hypothesize that TDP-43 RNP granules in the axon display liquid droplet behaviors. If this hypothesis is true, then compared with membrane-bound axonal cargos, RNP granule motility will show distinct properties, including (*i*) an ability to interact with other RNA granules to influence trajectory and composition, (*ii*) frequent fusion events with rapid relaxation to spherical shape, (*iii*) deformability by shear stress, (*iv*) rapid internal redistribution, and (*v*) sensitivity to disruption of weak hydrophobic interactions. In addition, we predict

Significance

Mutations in TAR-DNA binding protein 43 (TDP-43), an RNA-binding protein (RBP) with multiple functions in RNA metabolism, cause amyotrophic lateral sclerosis (ALS), but it is uncertain how defects in RNA biology cause disease. Purified RNA-binding protein FUS and heterogeneous nuclear ribonucleoprotein A1 (hnRNP A1) form liquid droplets in vitro through liquid–liquid phase separation. However, the biophysical properties of ribonucleoprotein (RNP) granules composed of wild-type (WT) or ALS-linked TDP-43 have not been studied in primary neurons. We show that TDP-43 WT RNP granules exhibit distinct biophysical properties depending on their axonal location, whereas granules formed by ALS-linked mutant TDP-43 are more viscous and show disrupted axonal transport dynamics. We propose the distinct biophysical properties of these neuronal RNP granules may reflect different maturational states and differential propensity for pathological transformation.

Author contributions: P.P.G., J.J.N., and E.L.F.H. designed research; P.P.G., J.J.N., and E.K. performed research; J.J.N. contributed new reagents/analytic tools; P.P.G., J.J.N., and E.L.F.H. analyzed data; P.P.G. and E.L.F.H. wrote the paper; and J.J.N. performed stimulated emission depletion microscopy and computational image analysis.

The authors declare no conflict of interest.

This article is a PNAS Direct Submission.

[1]To whom correspondence should be addressed. Email: holzbaur@mail.med.upenn.edu.

This article contains supporting information online at www.pnas.org/lookup/suppl/doi:10.1073/pnas.1614462114/-/DCSupplemental.

that ALS-linked mutations in the glycine-rich C-terminal domain of TDP-43 would alter the viscoelastic properties of RNP granules.

Here, we show that TDP-43, as a component of neuronal RNP transport granules, displays liquid-like properties in the axons of primary neurons. Moreover, wild-type (WT) neuronal TDP-43 RNP transport granules exhibit distinct biophysical properties in the proximal and middle (mid) axon, indicating granule properties are dependent on subcellular context and alter over time. Further, we find that disease-linked TDP-43 mutant granules display increased viscosity compared with TDP-43 WT. The diverse biophysical properties observed for neuronal RNP granules may represent different maturational states and/or contribute to differential propensity for pathological transformation.

Results

Distinct Populations of TDP-43 RNP Granules in the Proximal and Mid Axon. We reasoned that if TDP-43 forms liquid-like RNP granules in neurons, then the neurons should demonstrate motility characteristics and biophysical properties distinct from the characteristics and properties exhibited by membrane-bound organelles. We expressed EGFP- or Halo-tagged human TDP-43 WT in rat primary cortical neurons either alone or in combination with RFP-LAMP1 or DsRed2-Mito. Exogenous expression of TDP-43 WT mirrors endogenous TDP-43, with predominant nuclear localization and punctate axonal expression (Figs. S1 *A*, *Left* and *B*). In agreement with previous work that showed TDP-43 cotransports with *Nefl* mRNA (26), most TDP-43 granules in neuronal processes are positive for Syto select RNA dye (Fig. S1*A*, *Center*). Furthermore, axonal TDP-43 puncta are not observed in cortical neurons expressing mutant TDP-43 that has F-to-L substitutions in both RRMs, and therefore cannot bind RNA (23, 32), suggesting mRNA binding may be a prerequisite for TDP-43 RNP granule formation in neuronal axons (Fig. S1 *C* and *D*).

Motile TDP-43 RNP granules were transported for cumulative distances ranging from 10 to 130 μm and displayed instantaneous and net velocities consistent with motor-based fast axonal transport, as previously noted (25, 26). Instantaneous velocities reflect periods of oscillatory motility and/or short runs with frequent pauses, as well as periods of processive transport; 54% and 46% of motile granules showed net anterograde and retrograde displacement, respectively (Fig. S2). We observed that 21 ± 2.9% of axonal TDP-43 RNP granules underwent long-range transport (net displacement ≥ 10 μm), whereas a significant proportion of axonal TDP-43 RNP granules were stationary (<5 μm cumulative displacement) or showed oscillatory behavior (Fig. 1 *A*–*D*).

Focusing on the motile subpopulation of axonal TDP-43 RNP granules, we noticed that the majority of motile granules were located in the mid axon, defined as >50 μm from the cell soma. Conversely, the proximal axon contains twofold more stationary TDP-43 granules (45 ± 8.5%) than the mid axon (20 ± 4.0%; $P = 0.013$; Fig. 1*E*). This observation suggests that distinct populations of TDP-43 RNP granules may exist in the proximal vs. mid axon.

Compared with Membrane-Bound Organelles, TDP-43 RNP Granules Show More Frequent Interactions with Subsequent Changes in Trajectory. While analyzing TDP-43 RNP granule motility, we observed frequent interactions between adjacent granules, including fusion events and more transitory interactions that often were followed by a change in trajectory (Fig. 1*F* and Fig. S3). Although membrane-bound organelles, such as mitochondria and endosomes/lysosomes, can also fuse, we asked whether the frequency of interactions with a subsequent change in trajectory was significantly different between membrane-bound organelles and TDP-43 WT RNP granules. We examined interactions between TDP-43, LAMP1, or mitochondria, and using specific criteria (*SI Materials and Methods*), we scored each interaction as resulting in "change" or "no change" in trajectory. TDP-43 interactions were followed by a trajectory change in 12 of 32 interactions, whereas only three of 32 LAMP1 interactions and two of 31 mitochondrial interactions were followed by a trajectory change (χ^2 test, $P = 0.0017$). Thus, TDP-43 interactions result in significantly different behavior compared with membrane-bound organelles, such as LAMP1$^+$ vesicle or mitochondrial interactions (Fig. 1 *F* and *G*).

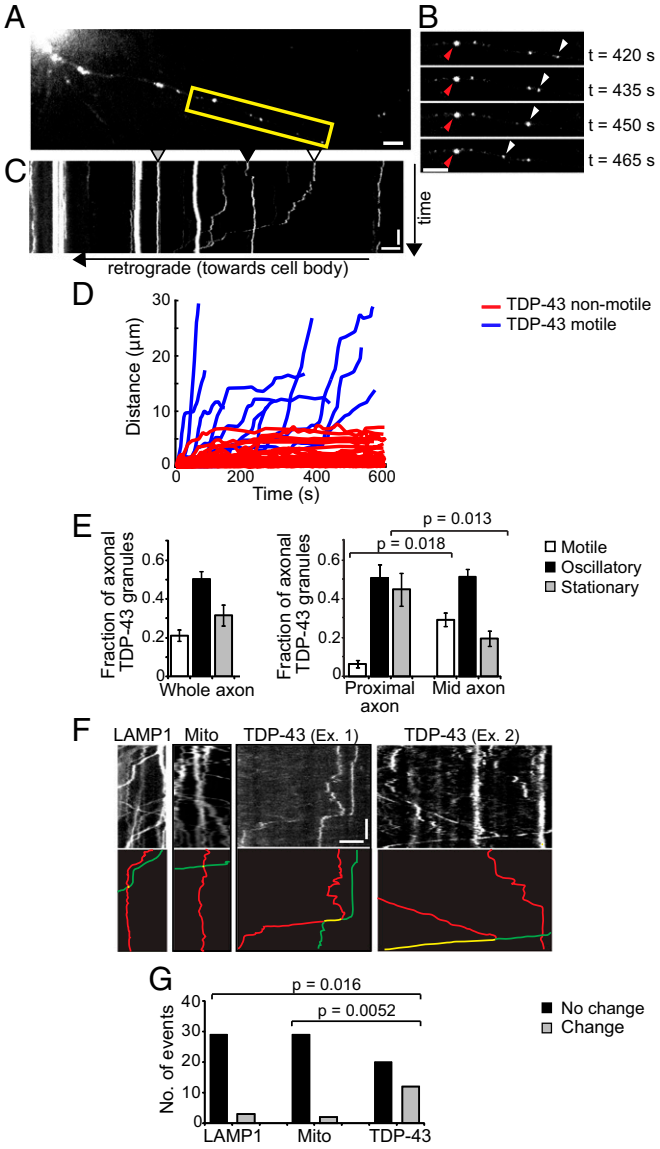

Fig. 1. Axonal TDP-43 RNP granule interactions often result in trajectory changes. (*A*) TDP-43 granules are observed along the axon of a primary cortical neuron (days in vitro 7–10) expressing EGFP–TDP-43 WT. The boxed area is enlarged in *B*. (*B*) Time-lapse images of a stationary TDP-43 granule (red arrowhead) and a motile TDP-43 granule (white arrowhead) at 15-s intervals. (Scale bars: *A* and *B*, 5 μm.) (*C*) Kymograph shows representative stationary (gray arrowhead), oscillatory (black arrowhead), and motile (white arrowhead) TDP-43 granules. (Scale bars: 5 μm and 100 s.) (*D*) Distance vs. time plot of representative motile TDP-43 granules; motile puncta show ≥10 μm net displacement in 10 min. (*E*) Fraction of axonal TDP-43 granules that are stationary, oscillatory, or motile (*Left*), binned according to location in the proximal or mid axon (*Right*) (mean ± SEM). ANOVA was performed, with a Tukey posttest ($n = 17$ neurons, four independent experiments). (*F*) Kymographs showing representative interactions between LAMP1 vesicles (*Left*), mitochondria (*Center*), and TDP-43 granules (*Right*). Intersecting tracks are highlighted in red and green below each kymograph, and interactions between tracks are highlighted in yellow. (Scale bars: 5 μm and 60 s.) (*G*) Interactions between LAMP1 vesicles ($n = 32$ interactions from 16 kymographs), mitochondria ($n = 31$ interactions from 16 kymographs), or TDP-43 granules ($n = 32$ interactions from 16 kymographs) that result in a change (gray bars) or no change (black bars) in trajectory following the interaction (χ^2 test, $P = 0.0017$). A Fisher exact test with Bonferroni correction for multiple comparisons was performed, where $P = 0.025$ was used as the significance threshold.

TDP-43 RNP Granules Dynamically Change Composition via Fusion and Fission Events. Because TDP-43 RNP granule interactions more often result in directional or motility changes compared with interactions between membrane-bound organelles, we asked whether these contact events between TDP-43 RNP granules alter granule composition, facilitating exchange of proteins. To address this question, we took two complementary approaches. First, we live imaged neurons coexpressing low levels of EGFP- and Halo-tagged TDP-43 WT in varying ratios. This approach resulted in stochastic differential labeling in a subset of granules and allowed us to identify fusion events (*SI Materials and Methods*). We also used photobleaching experiments to demonstrate transference of fluorescence intensity from nonbleached TDP-43 WT RNP granules to a bleached granule. Using the first approach, we observed fusion and mixing of differentially tagged TDP-43 RNP granules (Fig. S3 *A–C* and Movie S1). Interacting granules demonstrate reciprocal changes in the intensity ratio of Halo/EGFP (Fig. S3*C*). In addition, we observed fission of TDP-43 RNP granules containing both EGFP–TDP-43 and Halo–TDP-43; deformation of the granule precedes splitting into two "daughter" granules, each with a distinct Halo/EGFP ratio (Fig. S4).

Using the photobleaching approach, we observed successive interactions between granules that result in transference of fluorescence intensity from neighboring nonbleached TDP-43 RNP granules (Fig. 2 and Movie S2, pink and green arrowheads) to a bleached TDP-43 RNP granule (Fig. 2 and Movie S2, blue arrowhead). While interacting with the first nonbleached TDP-43 granule (Fig. 2 and Movie S2, pink arrowhead; 5 s postbleach), the bleached TDP-43 granule gains ≈25% fluorescence intensity (ΔI, interaction 1). Similarly, the bleached TDP-43 granule gains ≈20% fluorescence intensity (ΔI, interaction 2) after interacting with the second nonbleached granule (Fig. 2 and Movie S2, green arrowhead; 10 s postbleach). There are corresponding reductions in the fluorescence intensity of the donating TDP-43 RNP granules (Fig. 2*B*). Together, these data indicate that TDP-43 RNP granules in neurons undergo fusion and fission events similar to other types of RNP structures (2, 3, 6), but also undergo more transient interactions that mediate exchange of RBPs, specifically TDP-43, between RNP granules.

Neuronal TDP-43 RNP Granules Display Liquid-Like Properties in the Axon. The dynamic nature of axonal TDP-43 RNP granules, specifically fusion events, is highly suggestive of a liquid droplet state, and these liquid-like behaviors are similar to those behaviors observed for P granules, nucleoli, and stress granules (1–3, 6). Three main characteristics define a phase-separated liquid-like compartment: (*i*) liquid droplets should be roughly spherical due to surface tension but will deform under shear stress, (*ii*) two liquid droplets will fuse into single circular droplet with a characteristic relaxation time, and (*iii*) liquid droplets undergo rapid internal rearrangements (5, 8, 33). We asked whether TDP-43 RNP granules in the axon display these liquid-like biophysical properties.

Confocal microscopy demonstrates that TDP-43 RNP granules are roughly circular at rest, with an aspect ratio (AR; maximal diameter/minimal diameter) of 1.18 ± 0.09 (mean ± SEM), in agreement with a liquid droplet state (Fig. 3*A*). Simple Newtonian liquids suspended in another fluid of lower viscosity (i.e., the cytoplasm) will deform in response to shear stress, unlike an elastic solid, which maintains memory of its prior shape (5, 33, 34). The degree of deformation depends on both the magnitude of shear stress as well as the viscoelastic properties of the liquid. If this assumption is true for TDP-43 granules, then we would expect to observe transient shape changes during fast axonal transport and relaxation back to the lowest energy (circular) form when transport stops. In contrast, membrane-bound organelles, particularly those organelles with a rigid internal structure, are not expected to show significant alterations in shape.

We used near-total internal reflection fluorescence (near-TIRF) microscopy to live-image transport of TDP-43 granules, mitochondria, and LAMP1 vesicles in the axon with a higher degree of temporal resolution (seven to 10 frames per second). As expected, membrane-bound organelles, such as mitochondria and LAMP1 vesicles, did not show significant alterations in shape during transport (Fig. 3*A* and Fig. S5). We observed that TDP-43 granules underwent dramatic shape deformation during axonal transport at instantaneous velocities

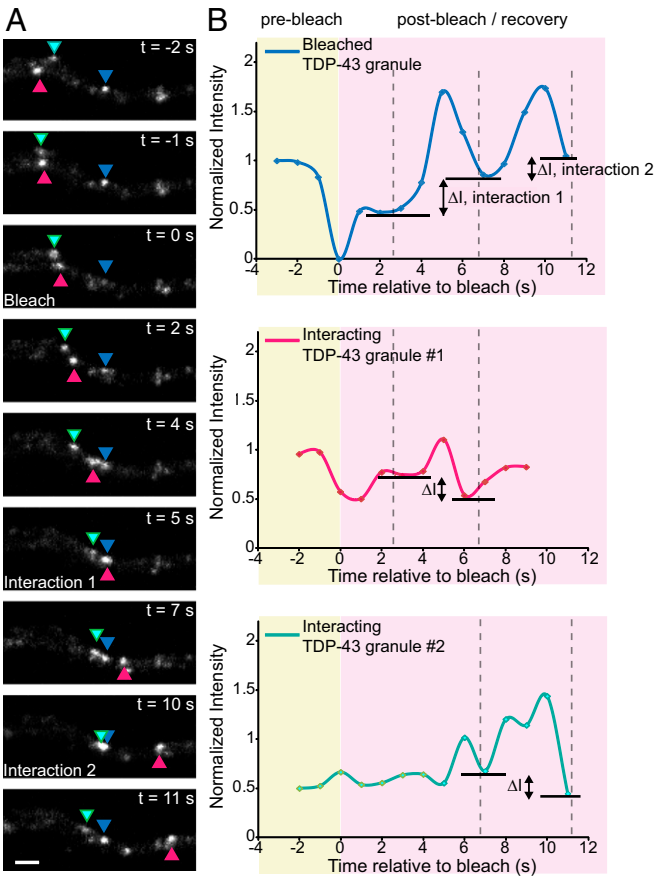

Fig. 2. Interactions between TDP-43 granules facilitate transfer of material between granules. (*A*) Photobleaching experiments demonstrate transference of fluorescence intensity from nonbleached TDP-43 RNP granules to a bleached granule. A single axonal TDP-43 granule was photobleached (blue arrowhead) at time (t) = 0 s in a cortical neuron transfected with EGFP–TDP-43. Two distinct nonbleached TDP-43 granules interact with the bleached granule at t = 5 s (pink arrowhead) and at t = 10 s (green arrowhead) (also Movie S2). (Scale bar: 2 μm.). (*B*) Normalized intensities of the bleached TDP-43 granule (blue line), nonbleached interacting granule 1 (pink), and nonbleached interacting granule 2 (green) are plotted as a function of time. With each interaction, the bleached granule gains intensity (ΔI), and there is a corresponding loss of intensity from each of the "donating" nonbleached granules. The solid lines represent spline fits of the data.

>3 μm·s^{-1} (AR = 1.79 ± 0.2; $P < 0.001$). More modest deformation (AR = 1.58 ± 0.2) occurred at instantaneous velocities ≤3 μm·s^{-1}.

Furthermore, a simple Newtonian liquid droplet that deforms under shear stress while suspended in a lower viscosity fluid will relax to the lower energy spherical shape with a characteristic time constant: $\tau_{relax} \sim L(\eta/\gamma)$; this relaxation constant depends on the viscoelastic properties of the liquid (η), droplet size (L), and surface tension between the two fluids (γ) (1, 2, 33). If TDP-43 RNP granules are liquid droplets, then we would expect a deformed TDP-43 granule to relax back to a circular shape as its instantaneous velocity approaches zero. Indeed, we identified several examples in which we observed slowing of transport and simultaneous relaxation of the deformed TDP-43 granule back to a circular AR (Fig. 3*B*). These data best fit a double exponential, with a fast relaxation phase ($\tau 1_{relax}$ = 0.19 s) that may reflect a rapid "snap-back" following cytoskeletal release (35) and a second slower relaxation phase ($\tau 2_{relax}$ = 3.4 s) that may reflect the viscoelastic properties of TDP-43 granules (Table S1).

Frequent fusion events with characteristic relaxation to a spherical shape are another property of liquid droplets. The fusion of nucleoli and yeast P bodies occurs over a time scale of minutes and seconds, respectively (2, 3). Using confocal microscopy, we had noticed fusion

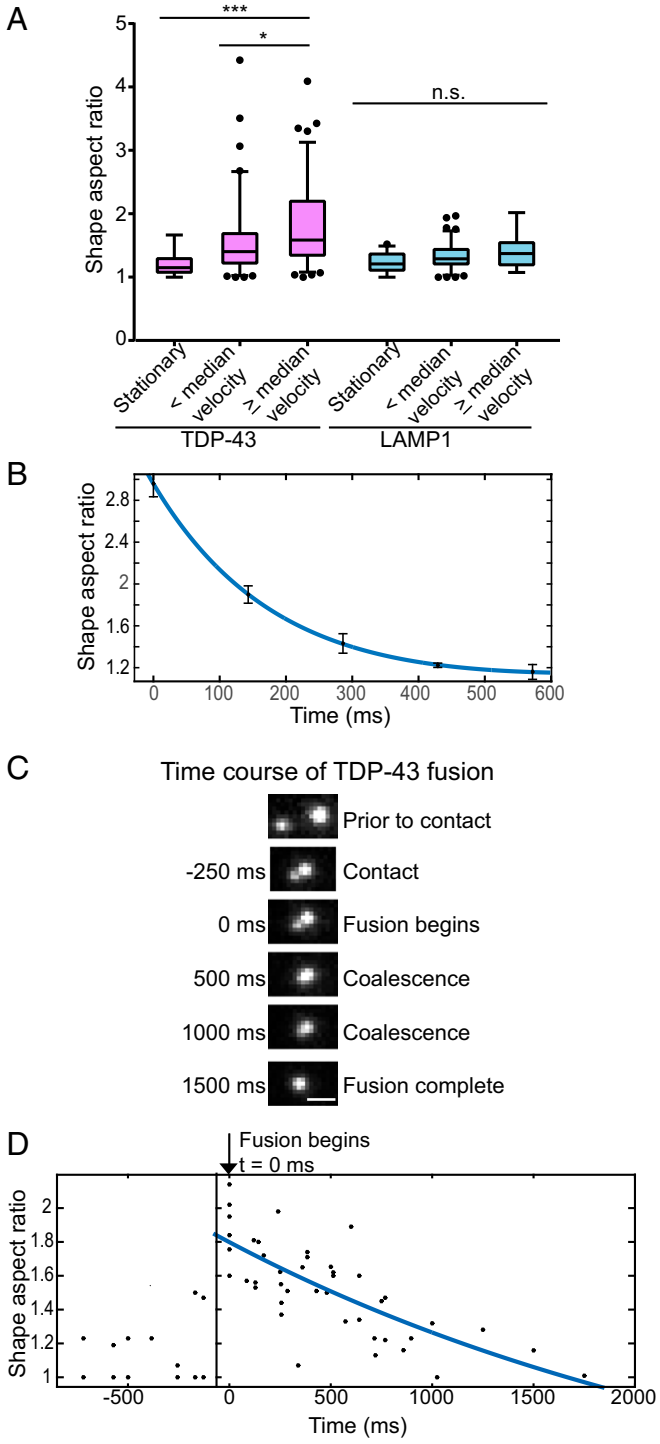

Fig. 3. TDP-43 RNP granules show liquid-like behaviors. (*A*) TDP-43 granules (purple bars) deform with increasing instantaneous velocity, as assessed by AR (maximum diameter/minimum diameter). TDP-43 granules moving at speeds above the median instantaneous velocity show statistically significant deformation compared with stationary TDP-43 granules (***$P < 0.001$, ANOVA with Tukey posttest). In contrast, LAMP1 vesicles (blue bars) do not significantly change shape regardless of instantaneous velocity. n.s., not significant. AR was measured from nine representative TDP-43 granules from five neurons over four independent near-TIRF live-imaging experiments, including at stationary time points ($n = 12$) and at below ($n = 84$) and above ($n = 90$) the median instantaneous velocity. LAMP1 AR measurements were obtained from nine representative vesicles from eight neurons over three independent experiments, including stationary vesicles ($n = 34$) and vesicles transported below ($n = 87$) and above ($n = 87$) the median velocity. (*B*) Deformed TDP-43 granules undergo characteristic relaxation to a circular shape upon slowing of transport (defined as $t = 0$ s), with fast ($\tau 1_{relax} = 0.19$ s) and slower ($\tau 2_{relax} = 3.4$ s) relaxation phases. Plotted data represent mean ± SEM ($n = 5$ deformation events; Table S1). (*C* and *D*) Near-TIRF microscopy was used to observe fusion events between TDP-43 granules and to capture the relaxation of two TDP-43 granules into a single circular granule (also Movie S3). (Scale bar: 0.5 μm.) Shape AR was plotted as a function of time, where t = 0 ms was the point of contact between the two fusing TDP-43 granules ($n = 6$ fusion events from four neurons); negative values for time refer to time points before contact between fusing TDP-43 granules ($\tau_{relax} = 2.7$ s; Table S1).

between TDP-43 RNP granules (Fig. 1*F* and Fig. S3), but these fusion events occurred rapidly, over milliseconds to seconds. To obtain better temporal resolution of fusion events (seven to 10 frames per second), we again used near TIRF microscopy. Fusion of two TDP-43 granules begins with an initial contact event and an elongated shape AR, which rapidly relaxes into a circular AR (Fig. 3 *C* and *D* and Movie S3). This relaxation curve is best fit with a single exponential, with characteristic τ_{relax} of 2.7 s (Table S1). The relaxation constant of two fusing TDP-43 granules is similar to the slower phase of relaxation ($\tau 2_{relax} = 3.4$ s) calculated above for relaxation of deformed TDP-43 granules.

TDP-43 RNP Granules Along the Mid Axon Show Rapid Fluorescence Recovery After Photobleaching. If TDP-43 RNP granules represent liquid droplets, there should be constant mixing of TDP-43 molecules within RNP granules as well as exchange with the cytoplasmic pool of TDP-43. We tested these predictions by measuring fluorescence recovery after photobleaching (FRAP) of whole EGFP–TDP-43 granules or approximately half of a granule ("half-bleach") (1). We also compared fluorescence recovery of TDP-43 with fluorescence recovery of mitochondria and LAMP1 vesicles (Fig. S6). FRAP of axonal TDP-43 RNP granules is technically difficult due to their small size and motility (36). As a result, we performed predominantly whole-bleach experiments in mid axonal TDP-43 granules ($n = 16$), but we also were able to half-bleach a limited number of mid axonal TDP-43 granules ($n = 4$). We could more easily half-bleach TDP-43 granules in the proximal axon ($n = 10$), where the granules were more likely to be stationary (Fig. 1*E*).

In the mid axon, whole-bleach analysis of TDP-43 granules demonstrates 100% recovery of fluorescence intensity on the order of seconds and suggests that TDP-43 granules exist in dynamic equilibrium with the cytoplasmic pool of unbleached TDP-43 (Fig. 4 *A* and *D*) ($\tau = 11.2$ s; Table S2). However, we cannot exclude some contribution of reversible photobleaching of EGFP to the observed recovery (37).

Similarly, half-bleached TDP-43 granules in the mid axon demonstrated rapid redistribution and 100% recovery of fluorescence intensity in the bleached area (Fig. 4 *B* and *D* and Table S2). In contrast, proximal TDP-43 granules that were half-bleached only recovered 30% of prebleach fluorescence intensity (Fig. 4 *C* and *D*). The fluorescence recovery curve for proximal axon TDP-43 granules was best fit with a double exponential equation ($\tau 1 = 1.43$ s and $\tau 2 = 19.8$ s; Table S2) and suggests that proximal TDP-43 granules have a small mobile fraction that rapidly recovers fluorescence as well as a more viscous or less dynamic stabilized region that does not readily mix with adjacent areas within the granule or exchange with soluble TDP-43. Recovery of fluorescence intensity in half-bleached TDP-43 RNP granules occurred, at least in part, through redistribution of TDP-43 from the unbleached area to the bleached area. As the bleached area recovers, there is a corresponding loss of fluorescence intensity in the unbleached area (Fig. 4 *E*–*G*). These observations suggest a high degree of internal mobility within TDP-43 RNP granules and are consistent with a liquid state.

Using the proximal and mid axon half-bleach time constants and estimated bleach radius (*SI Materials and Methods*), we approximated the diffusion coefficient (DC) of EGFP–TDP-43 within proximal and mid axonal RNP granules (38) (Table S2). We assumed that TDP-43 RNP granules act as equilibrium Newtonian liquids and used the DC values in the Stokes–Einstein relationship to calculate TDP-43 granule viscosity (η), as previously described (1). Mid axon TDP-43 granules had an estimated viscosity of $\eta \sim 0.1$ Pa·s^{-1}, which is ~100-fold more

viscous than water. Proximal axon TDP-43 granules appeared to be more complex because the estimated viscosity of the rapidly recovering mobile fraction was $\eta \sim 0.01$ Pa·s^{-1}, whereas the less dynamic portion had an estimated viscosity of $\eta \sim 3.7$ Pa·s^{-1}. These data suggest proximal TDP-43 RNP granules are biophysically distinct from mid axon granules and are composed of a dynamic, liquid-like phase but also more stabilized or "solid-like" areas with limited molecular mobility.

Superresolution Microscopy Demonstrates Enhanced RNP Granule Density and Irregular Granule Morphology in the Proximal Axon. We next asked whether TDP-43 granules in the proximal axon have distinctive morphological or size characteristics that may provide insight into the distinct bleach recovery characteristics of proximal and mid axon TDP-43 granules. Stimulated emission depletion (STED) superresolution microscopy revealed only small differences in the cross-sectional area of endogenous TDP-43 RNP granules based on axonal location (proximal axon: 0.024 ± 0.003 μm^2, mid axon: 0.025 ± 0.003 μm^2; Fig. 5 *A* and *C*). Exogenously expressed EGFP–TDP-43 granules show a similar size distribution (Fig. 5 *B* and *D*). However, STED microscopy showed a two- to threefold greater density of TDP-43 granules in the proximal axon than in the mid axon, both for endogenous TDP-43 in primary cortical neurons and in neurons expressing EGFP–TDP-43 at low levels (Fig. 5*E* and Fig. S7). We also performed nearest neighbor distance (NND) calculations on STED images and determined the distance from each granule to its five nearest neighbors. We found that the average NND in the proximal axon [1,210 ± 66 nm (mean ± SEM)] is significantly less than in the mid axon (2,320 ± 350 nm; Fig. S7*D*).

Recent studies in vitro have shown that several factors, including RBP concentration, molecular crowding agents, salt concentration, and presence or absence of RNA, all influence the propensity for LLPS and alter the viscous properties of RNP granules (6, 13–16, 39, 40). Consistent with these findings, our STED density and NND data suggest that TDP-43 is more concentrated in the proximal axon and that compartment-specific differences in the local concentration of TDP-43, and possibly other RBPs, may contribute to the biophysical differences we observed in proximal and mid axonal TDP-43 RNP granules.

"Aging" and repeated phase cycling of purified FUS and hnRNP A1 in vitro also induce morphological and biophysical changes, such that some droplets lose their spherical shape and acquire an angulated or starburst appearance (6, 15, 16, 18). Morphologically, we observed that proximal TDP-43 granules possess more irregular contours compared with mid axonal granules (Fig. 5*F*). Population analysis of granule shape and morphology from STED images revealed that proximal TDP-43 granules have a significantly lower circularity and convexity ratio than mid axonal TDP-43 granules (Fig. 5 *G* and *H*).

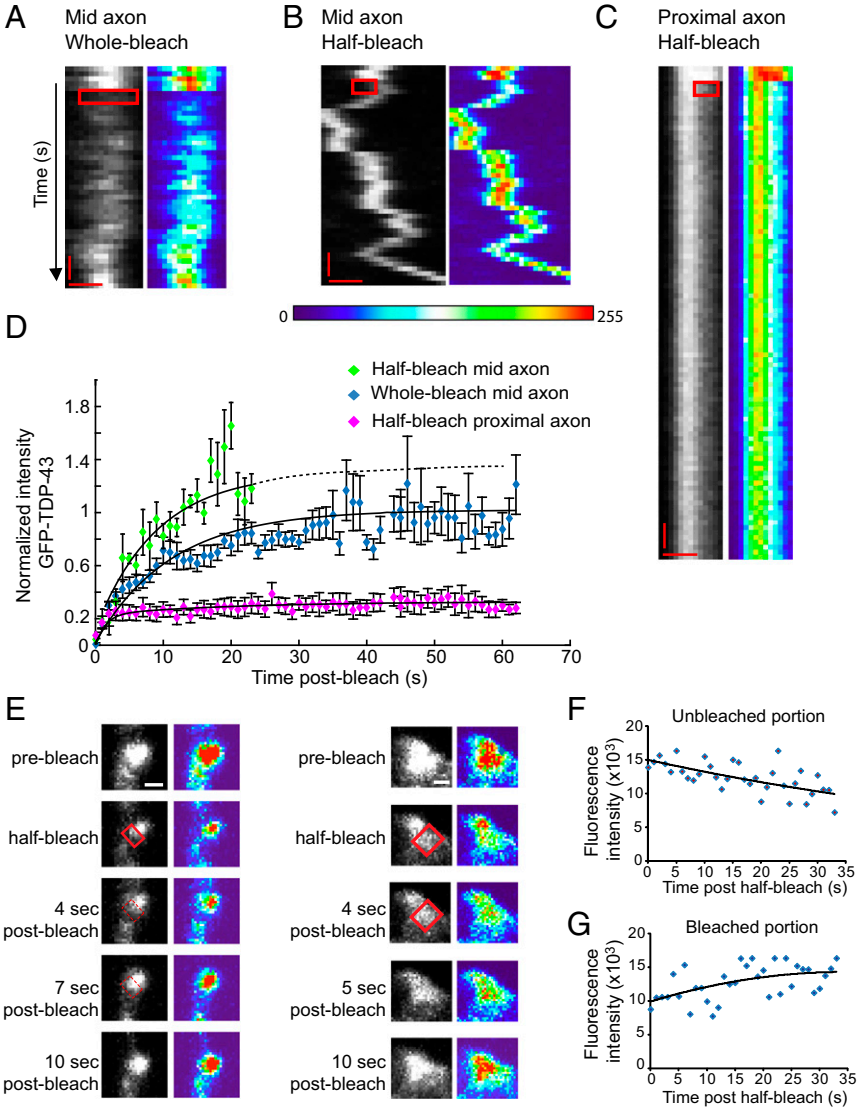

Fig. 4. FRAP identifies distinct populations of axonal TDP43 granules. TDP-43 granules in the mid axon display rapid recovery after whole-bleach (*A*) and half-bleach (*B*) experiments, suggesting that both reorganization within TDP-43 granules and dynamic exchange between granules and the soluble pool of TDP-43 occur. (*C*) Proximal axon TDP-43 granules show incomplete recovery after half-bleach. In *A*–*C*, rectangular boxes highlight the bleached area. (Scale bars: 0.5 μm and 5 s.) (*D*) Fluorescence recovery curves for proximal TDP-43 granules (n = 10) and for mid axon whole-bleach (n = 16) and half-bleach (n = 4) experiments. The normalized intensity values for each condition represent mean ± SEM. Solid lines represent best-fit exponential curves for each condition. Data were obtained from at least four independent experiments. (*E*, *Left*) Half-bleach of a representative mid axonal TDP-43 granule demonstrates rapid internal mobility and recovery of fluorescence intensity; however, the size of the granule limits the ability to visualize this redistribution of fluorescence within the granule. (*E*, *Right*) Therefore, a larger half-bleached TDP-43 granule is also shown, which demonstrates loss of fluorescence intensity in the unbleached region as the bleached region recovers. In the heat maps, red denotes high intensity and blue represents background intensity. (Scale bars: 0.5 μm.) There is loss of fluorescence intensity in the unbleached area shown in *E* (*F*), whereas the bleached area recovers intensity (*G*). Solid lines represent best-fit curves.

Taken together, the motility, FRAP, and superresolution morphology data suggest that proximal TDP-43 RNP granules are less motile, are less dynamic after photobleaching, and exhibit irregular contours; these features may reflect formation of stabilized regions within proximal TDP-43 granules.

To address whether proximal TDP-43 granules may be older or more "mature" than mid axonal granules, we used mEos3.2, a green-to-red photoconvertible fluorophore (41–43), tagged to TDP-43 WT to show that a photoconverted (red) pool of TDP-43 granules in the proximal axon largely "matures in place," whereas green (non-photoconverted) granules accumulate in the mid axon at later time points (Fig. S8 *A–D*). Although we cannot completely exclude the possibility that some of the proximal (red) granules had relocated from the mid axon before photoconversion, the data suggest that TDP-43 granules first entering the axon largely remain in the proximal axon, whereas newer granules are transported into the mid axon. In addition, the fluorescence recovery characteristics of proximal TDP-43 granules change with increasing time after transfection. Half-bleached proximal TDP-43 granules in the axon display robust fluorescence recovery at 15 h posttransfection, but show little recovery at 22–24 h posttransfection (Fig. 4 *C* and *D* and Fig. S8*E*). These data suggest maturation of TDP-43 granules and/or increasing TDP-43 expression levels could influence the biophysical characteristics of TDP-43 granules over time.

Mid Axon TDP-43 RNP Granules Are Sensitive to Disruption of Weak Hydrophobic Interactions. To test our hypothesis that granule properties are dependent on subcellular context, especially in morphologically complex cells, such as neurons, we compared the response of proximal and mid axon granules to chemical disruption. Recent studies have shown that the weak hydrophobic interactions between intrinsically disordered regions of RBPs underlie the dynamic biophysical properties of liquid droplet assemblies in vitro (6, 13–18) and in cells (3). To distinguish further the biophysical properties of proximal and mid axon TDP-43 granules, we treated neurons expressing EGFP–TDP-43 WT with 1,6-hexanediol, an aliphatic alcohol previously shown to disrupt weak hydrophobic interactions (44) and dissolve stress granules and P bodies in mammalian cells (3). Based on our photobleaching experiments, we hypothesized that weak hydrophobic interactions between TDP-43 molecules underlie the dynamic liquid-like properties of mid axon TDP-43 granules, which would be more susceptible to hexanediol, whereas TDP-43 granules in the proximal axon have less dynamic, more stabilized regions that would be less susceptible to chemical disruption. Consistent with this prediction, we observed that 1,6-hexanediol rapidly and reversibly dissolved TDP-43 granules in the mid axon but did not affect the integrity of proximal axon TDP-43 granules (Fig. 6). We also note that mid axon TDP-43 granules reform after 1,6-hexanediol washout, indicating they are more dynamic in both disassembly and reassembly. Together with data from photobleaching experiments, these observations suggest weak hydrophobic interactions maintain mid axon TDP-43 granules and underlie their dynamic liquid properties, whereas proximal axon TDP-43 RNP granules are maintained through more stabilized interactions that are potentially the result of time-dependent maturation.

ALS-Linked Mutations Disrupt TDP-43 RNP Granule Motility and Increase Granule Viscosity. Characterization of FUS and hnRNP A1 liquid droplets suggests disease-linked mutations accelerate transformation to a fibrillar state (6, 15, 16, 18). We hypothesized that ALS-linked mutations, M337V (27, 45) and G298S (46), in the LCS of TDP-43 would alter the liquid-like properties of axonal TDP-43 RNP granules and disrupt their function. Motile TDP-43 M337V and G298S granules display similar instantaneous velocities to motile TDP-43 WT granules but show less efficient transport, consistent with previous characterization of TDP-43 mutant motility (26, 47). We noted that processive transport of motile TDP-43 mutant RNP granules is more often interrupted compared with TDP-43 WT granules; TDP-43 mutant processive runs frequently stall or halt completely upon interaction with another granule (Fig. 7 *A–C*). As a consequence, mean squared displacement analysis demonstrates a processive motility pattern for TDP-43 WT, whereas both M337V and G298S mutant granules display subprocessive motility (Fig. 7*D*).

We asked whether increased viscosity of mutant RNP granules may contribute to the disrupted transport we observed. To test this hypothesis, we compared half-bleach fluorescence recovery of TDP-43 WT

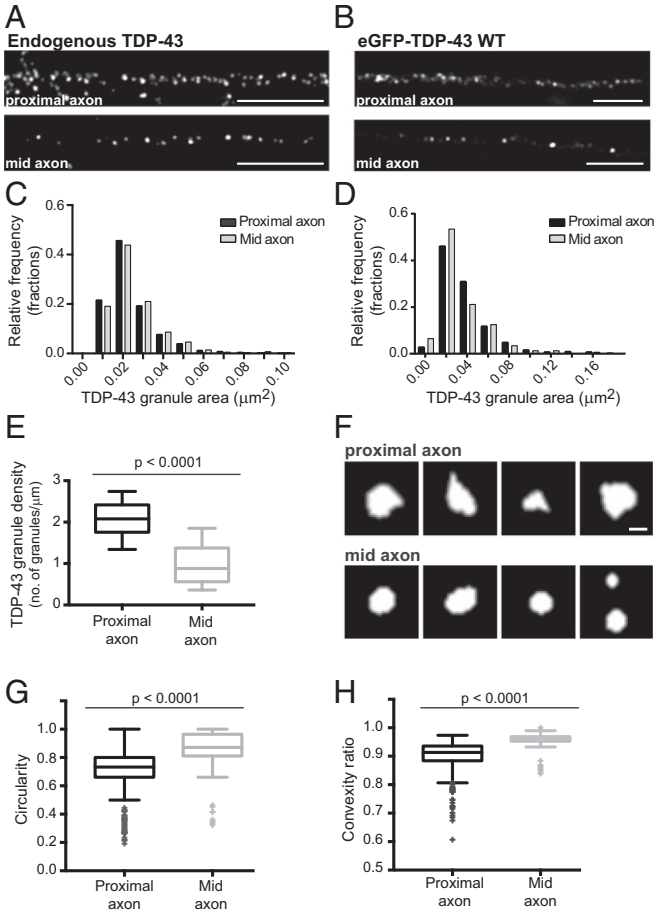

Fig. 5. Superresolution STED microscopy reveals proximal TDP-43 granules are less round, possess more irregular contours, and are distributed at a higher density compared with mid axonal granules. (*A*) Immunofluorescence for endogenous TDP-43 shows a higher density of TDP-43 granules in the proximal axon compared with the mid axon. (Scale bars: 2.2 μm.) (*B*) EGFP–TDP-43 in the proximal axon shows a higher density than in the mid axon. (Scale bars: 3 μm.) Images are maximum projections of deconvolved STED Z-stacks. (*C*) Size distribution of endogenous TDP-43 granules [proximal granule area: 0.024 ± 0.003 μm^2, mid axon granule area: 0.025 ± 0.003 μm^2 (mean ± SEM); n = 3,085 proximal granules and n = 776 mid axonal granules; Mann–Whitney test]. (*D*) Size distribution of EGFP–TDP-43 granules [proximal granule area: 0.036 ± 0.006 μm^2, mid axon granule area: 0.033 ± 0.007 μm^2 (mean ± SEM); n = 589 proximal granules and n = 232 mid axonal granules; Mann–Whitney test.] (*E*) EGFP–TDP-43 granule density was calculated for each axon segment imaged (n = 18 proximal axon, n = 13 mid axon). TDP-43 granule density in the proximal axon is significantly greater than in the mid axon (Student's t test, $P < 0.001$). (*F*) Proximal axon TDP-43 granules often display irregular contours and sharp projections, whereas mid axonal granules are usually round, with smooth borders. (Scale bar: 250 nm.) Images are segmented masks of TDP-43 granules. Mid axonal TDP-43 granules are significantly more circular (perfect circle, circularity = 1) (*G*) and have a significantly higher convexity ratio than proximal TDP-43 granules (*H*). Convexity is defined as the ratio of the object perimeter of the convex hull to the perimeter of the object (i.e., a convexity of a perfectly circular object is 1). Wilcoxon rank sum tests with a Bonferroni correction for multiple comparisons ($P \leq 0.001$) were performed to assess for significant differences in morphological features between proximal (n = 589) and mid (n = 232) axonal granules from 18 proximal axon and 13 mid axon images, respectively.

and mutant mid axon RNP granules. Both TDP-43 M337V and G298S granules show slower τ values and incomplete fluorescence recovery compared with TDP-43 WT granules (Fig. 7*E* and Table S2). Using the Stokes–Einstein equation, TDP-43 mutant granules show an order of magnitude increase (~20-fold) in viscosity compared with WT granules (Fig. 7*F* and Table S2). Compared with mid axonal TDP-43 WT granules, G298S and M337V TDP-43 granules are more resistant to 1,6-hexanediol (Fig. 7*G* and Fig. S9), suggesting these mutations in the glycine-rich C-terminal domain promote a stabilized internal structure. These data suggest ALS-linked mutations in TDP-43 disrupt normal transport granule function, but also possibly confer toxic gain of function by enhancing viscosity of mutant TDP-43 RNP granules.

Discussion

In this study, we examined TDP-43 RNP granule dynamics and their biophysical characteristics in neurons, which are morphologically complex and highly differentiated cells. Our data reveal properties that are both novel and not evident in vitro or in studies of RNP granules in cell lines. Recent studies have established that LLPS of purified FUS and hnRNP A1, and nuclear TDP-43, occurs in vitro and/or in mammalian cell lines (6, 15–17, 31). However, detailed characterization of TDP-43 has been limited due to its tendency to aggregate (15, 30). Here, we used live-cell and superresolution imaging techniques to show that TDP-43–positive neuronal RNP transport granules in the axon display biophysical properties consistent with liquid droplets, including fusion and fission events with characteristic relaxation to a spherical shape within seconds, deformability by shear force, rapid internal redistribution and FRAP, and sensitivity to disruption of weak hydrophobic interactions. Furthermore, we have identified distinct subpopulations of TDP-43 RNP granules according to axonal location (Fig. 8). Moreover, ALS-linked mutations in TDP-43 increase granule viscosity and disrupt transport function. We propose that the biophysical differences observed in TDP-43 RNP granules along the axon arise through differences in subcellular context and likely reflect maturational state, and, further, that ALS-linked mutations in TDP-43 may confer toxic gain-of-function effects on RNP granules, potentially increasing their propensity for pathological transformation.

Previous studies have demonstrated the liquid droplet properties of various types of cellular RNP granules and estimated their viscosity (η): *C. elegans* P granules, $\eta = 1$ Pa·s^{-1} (1); *X. laevis* oocyte nucleoli, $\eta = 10^3$ Pa·s^{-1} (2); and FUS-positive stress granules in HeLa cells, $\eta = 0.01$–0.1 Pa·s^{-1} (6) (Table S3). In vitro studies of purified WT FUS and *Ashbya gossypii* Whi3 protein have estimated comparable viscosities; moreover, these systems have allowed for various manipulations that alter the viscosity of these RBPs (18, 39). In our study, we have identified two populations of neuronal TDP-43 WT RNP granules, each with distinct biophysical properties. Mid axonal TDP-43 RNP granules are highly dynamic, motile, and susceptible to disruption by 1,6-hexanediol, suggesting they are held together by weak hydrophobic interactions. Accordingly, mid axonal TDP-43 granules show a high degree of internal molecular mobility as well as rapid exchange with the soluble pool of TDP-43. Mid axonal TDP-43 granules have a viscosity of 0.1 Pa·s^{-1}, which is ~100-fold more viscous than water and is comparable to the viscosity of FUS-positive stress granules in mammalian cells (6). In contrast, proximal TDP-43 granules show only partial FRAP, suggesting that they have a more limited mobile fraction and are less dynamic. Superresolution morphological analysis of axonal TDP-43 granules reveals that proximal TDP-43 granules are less circular and exhibit

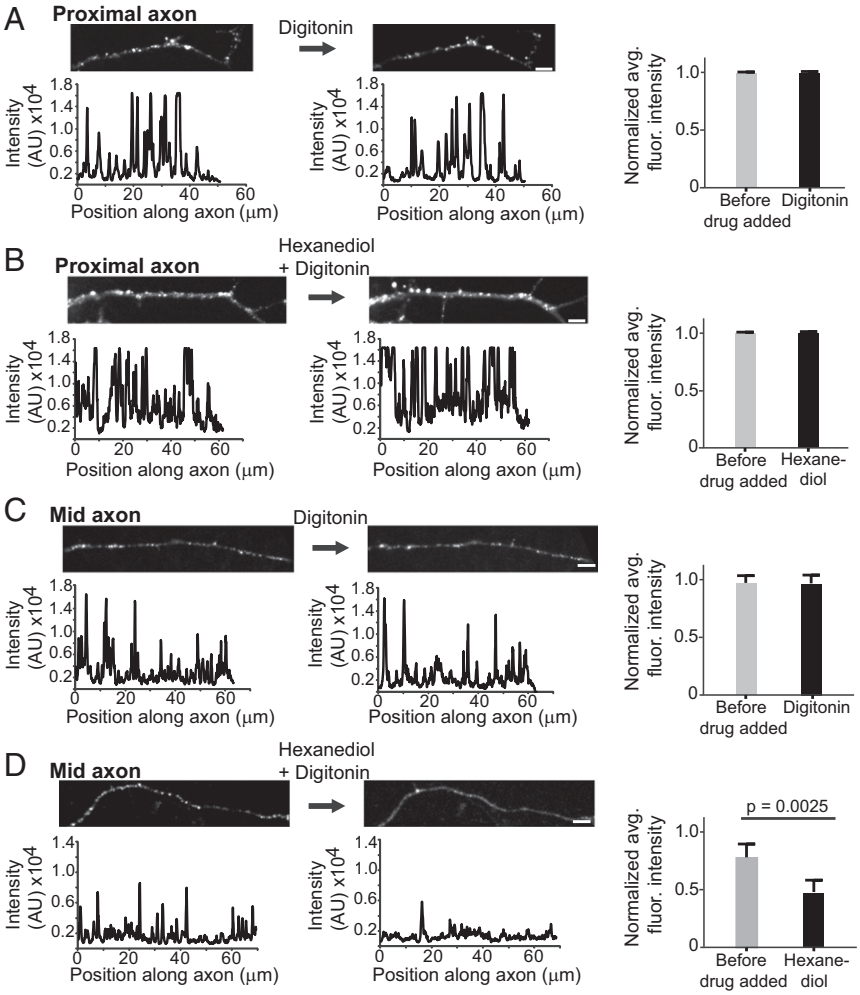

Fig. 6. Disruption of weak hydrophobic interactions dissolves TDP-43 granules in the mid axon but not in the proximal axon. Cortical neurons expressing EGFP–TDP-43 were treated with 5 μg/mL digitonin alone (control) or 5 μg/mL digitonin with 4% 1,6-hexanediol and then imaged at 5-min intervals. (*A* and *C*) Application of digitonin does not affect proximal or mid axonal TDP-43 granules. (*B* and *D*) Digitonin with 1,6-hexanediol dissolves TDP-43 granules in the mid axon but does not affect TDP-43 granule integrity in the proximal axon, as shown with representative images and intensity plot profiles (*Left*) and quantification of fluorescence (fluor.) intensity along the axon (*Right*) ($n = 15$ neurons per condition). (*D*) There is a significant reduction in fluorescence intensity in the mid axon with the addition of 1,6-hexanediol (Student's *t* test, $P = 0.0025$). (Scale bars: 5 μm.) AU, arbitrary units; avg., averaged.

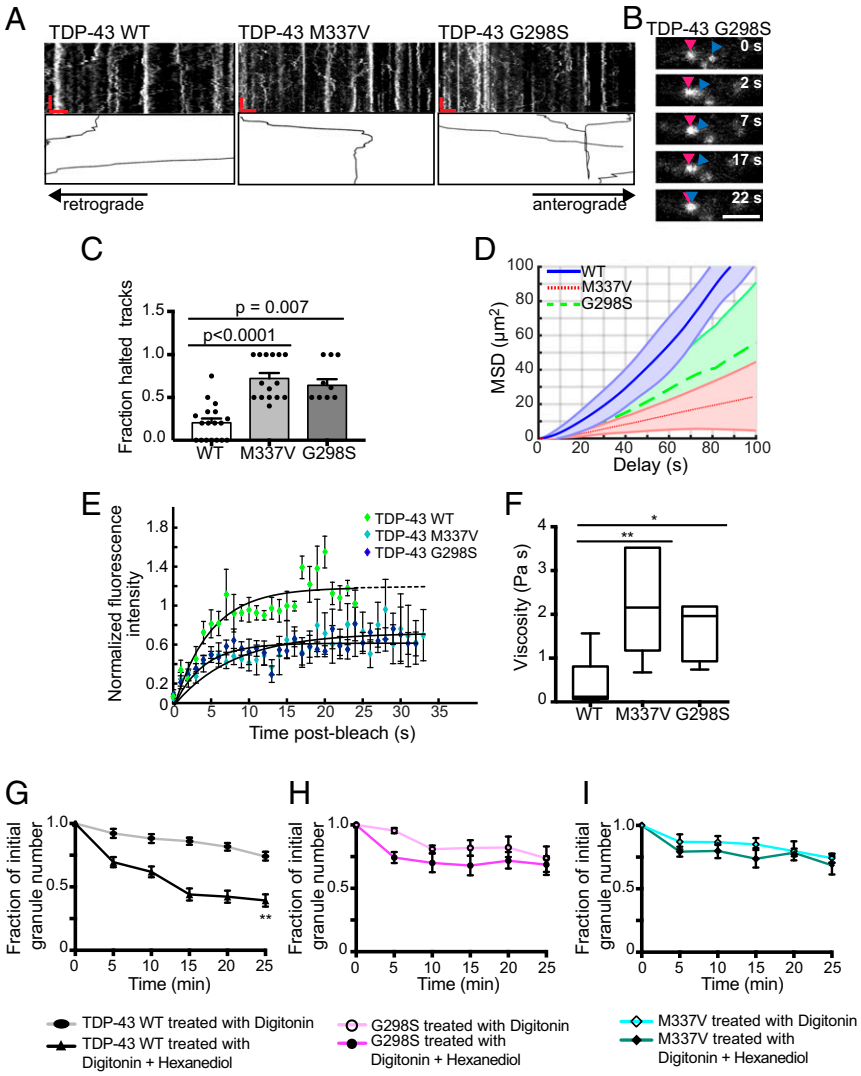

Fig. 7. ALS-linked mutant TDP-43 RNP transport granules show subprocessive motility and increased granule viscosity. (*A*) Representative TDP-43 WT, M337V, and G298S kymographs with motile, processive tracks traced. (Scale bars: 5 μm, 60 s.) (*B*) Time series of a TDP-43 G298S granule (blue arrowhead) that encounters a stationary granule (magenta arrowhead) and stops moving. (Scale bar: 2 μm.) (*C*) Significantly higher fraction of TDP-43 M337V and G298S motile, processive tracks show halting behavior compared with TDP-43 WT [Kruskal–Wallis test with Dunn's correction: TDP-43 WT (n = 20 neurons) and M337V (n = 15 neurons) from six independent experiments, G298S (n = 9 neurons) from three independent experiments]. (*D*) Mean squared displacement (MSD) analysis of the top 95th percentile of motile TDP-43 WT [diffusion coefficient (D) = 3.38 $\mu m^2 \cdot s^{-1}$, 95% confidence interval (CI): 3.2–3.6], M337V (D = 0.955 $\mu m^2 \cdot s^{-1}$, 95% CI: 0.93–0.98), and G298S (D = 1.52 $\mu m^2 \cdot s^{-1}$, 95% CI: 1.4–1.6) granules. Thicker lines represent mean MSD, and shaded areas represent SEM. Goodness of fit: TDP-43 WT, R^2 = 0.94; M337V, R^2 = 0.98; G298S, R^2 = 0.92; WT: n = 8 neurons; M337V: n = 7 neurons; G298S: n = 8 neurons; three independent experiments each. (*E*) Fluorescence recovery after half-bleach of mid axonal TDP-43 WT granules (n = 7), M337V (n = 6), and G298S (n = 6) from three or more independent experiments. Normalized intensity values represent mean ± SEM, and solid lines represent best-fit exponentials. (*F*) Mid axonal TDP-43 WT RNP granules are significantly less viscous (median = 0.099 $Pa \cdot s^{-1}$) than either TDP-43 M337V granules (median = 2.2 $Pa \cdot s^{-1}$; $^{**}P$ = 0.006, Kruskal–Wallis test with Dunn's correction) or G298S granules (median = 2.0 $Pa \cdot s^{-1}$; $^{*}P$ = 0.014, Kruskal–Wallis test with Dunn's correction). TDP-43 WT (n = 7), M337V (n = 6), and G298S (n = 6) from three or more independent experiments. TDP-43 WT (*G*), G298S (*H*), and M337V (*I*) TDP-43 granule number in the mid axon after 1,6-hexanediol treatment, compared with control conditions. Digitonin alone: WT (n = 15 neurons), G298S (n = 7 neurons), M337V (n = 10 neurons) from four independent experiments. Digitonin with hexanediol: WT (n = 17 neurons), G298S (n = 7 neurons), M337V (n = 10 neurons) from four independent experiments. ANOVA with a Tukey posttest was used for end-point analysis statistics ($^{**}P < 0.0001$). Error bars represent SEM.

irregular contours (Fig. 5 *E*–*G*). Thus, proximal TDP-43 granules appear to be more biophysically complex, with more stabilized regions not susceptible to disruption of weak hydrophobic interactions. Consistent with these interpretations, recent superresolution and proteomic characterization of mammalian stress granules suggests that these RNP granules also exhibit a stable substructure with a dynamic shell (48).

The biophysical differences between proximal and mid axon TDP-43 RNP granules may arise through several potential mechanisms. In vitro, FUS and hnRNP A1 display an intrinsic propensity for "maturation" to an oligomerized or fibrillized solid-like state (6, 14, 16, 18). Several lines of evidence suggest that the biophysical differences we found between proximal and mid axonal TDP-43 granules may also represent differences in their maturational states. In support of this possibility, we found that very few proximal TDP-43 granules escape into the mid axon, suggesting that most mature in place (Fig. S8 *A*–*D*). Consistent with this hypothesis, proximal TDP-43 granules exhibit fluorescence recovery characteristics that change over time. Proximal TDP-43 granules display complete half-bleach recovery at 15 h posttransfection (Fig. S8*E*). Over time, however, proximal TDP-43 granules transition to a less dynamic state (Fig. 4 *C* and *D* and Fig. S8*E*). Furthermore, just as "aged" FUS droplets in vitro develop a spiculated appearance (6),

STED superresolution microscopy revealed that in neurons, proximal axonal TDP-43 granules display irregular contours and spiculated edges and are less circular than mid axonal TDP-43 granules (Fig. 5 *F–H*). The intermolecular interactions that regulate granule maturation and formation of fibrillar and amyloid-like structures are not fully understood, but several factors may contribute, including molecular chaperones and high RBP concentrations within liquid-like droplets (16, 49).

Using STED superresolution microscopy, we see clear enrichment of endogenous TDP-43 in the proximal axon compared with the mid axon and a similar density gradient in neurons expressing EGFP–TDP-43 (Fig. 5 *A–E* and Fig. S7). Although additional evidence is needed, an interesting possibility is that the relative concentrations of TDP-43, and perhaps other RBPs, in different neuronal compartments allow for formation of RNP granules with distinct biophysical properties. Recent work has shown that RNA content influences the biophysical properties of liquid droplets as well (39, 40). For example, Zhang et al. (39) have shown that Whi3 RNPs become more viscous with increasing concentrations of RNA, and that addition of specific mRNA transcripts, *CLN3* and *BNI1*, involved in nuclear division and branching functions, respectively, result in Whi3 RNP granules with distinct viscosities.

A third possibility is that biophysical differences between proximal and mid axon TDP-43 RNP granules may reflect differences in their RNA content and could underlie distinct physiological functions. It has been shown recently that yeast stress granules are more gel-like, whereas P bodies have more liquid-like properties (3). Our motility data indicate that TDP-43 RNP granules in the mid axon are more likely to be transported distances ≥10 μm, suggesting that these granules may function to transport mRNAs critical for synaptic function or maintenance of the axon terminal (50, 51). Furthermore, weak hydrophobic interactions that maintain mid axonal TDP-43 granules as liquid droplets would allow for facile release of mRNA at the target site. In contrast, proximal TDP-43 RNP granules are predominantly stationary, and we speculate that distinct mRNAs may be associated with these granules. These findings raise the possibility that specific mRNAs are critical for creating biophysical diversity between cellular RNP granules and may drive unique biological functions; it will be important to examine this question in future studies.

In vitro, ALS/FTD-linked mutations in the RBPs FUS and hnRNP A1 do not significantly alter the biophysical properties of newly formed liquid droplets; rather, aging liquid droplets composed of mutant RBPs exhibit enhanced maturation to a more solid-like state with decreased molecular mobility (15, 16, 44). Cycling mutant hnRNP A1 or FUS through repeated rounds of LLPS promoted conversion of liquid droplets into fibrillar structures (15, 18). Previous studies have demonstrated ALS-linked mutations in TDP-43 accelerate its propensity to aggregate (30). In neurons, we observe that mid axonal granules composed of ALS-linked mutant TDP-43 show lower internal molecular mobility than TDP-43 WT granules (Fig. 7*E*); accordingly, mutant granules are ∼20-fold more viscous that WT granules (Fig. 7*F*). In addition, we and others have observed that ALS-linked mutations disrupt TDP-43 RNP transport (26, 47). These data suggest the altered viscoelastic properties of mutant TDP-43 granules may contribute to disease pathogenesis.

In this study, we show that neuronal TDP-43 RNP transport granules display liquid-like properties within cortical neurons, and thus provide insights that extend recently proposed models that suggest RNP granules are biophysically specialized structures fundamental for cellular compartmentalization. Our data demonstrate distinct biophysical properties of TDP-43 WT RNP granules depending on axon location. Further, we find that granules formed from ALS-linked mutant TDP-43 are more viscous and exhibit altered transport dynamics. Thus, our data indicate that RNP granules must be studied within the complex morphology of neurons to appreciate fully their physiological roles and the pathological transitions of these structures in neurodegenerative disease.

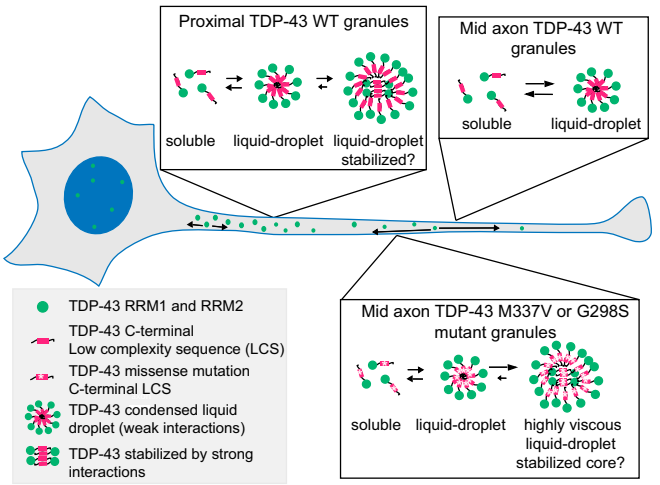

Fig. 8. Summary schematic: Mid axonal TDP-43 granules comprise a dynamic population of RNP granules that are distinct from proximal TDP-43 granules. Mid axonal TDP-43 RNP granules show rapid exchange with the soluble pool of TDP-43, display rapid internal rearrangement, and readily dissolve when weak hydrophobic interactions are disrupted, consistent with liquid-like behavior. In contrast, proximal TDP-43 granules show incomplete FRAP and are less sensitive to disruption of weak hydrophobic interactions, suggesting that these granules have a complex structure composed of more viscous and/or stabilized regions with limited molecular mobility. In addition, TDP-43 RNP granules are more densely arranged in the proximal axon and are less motile than mid axonal TDP-43 granules. These distinct populations of TDP-43 WT granules in the axon may reflect different maturational states, and possibly different functional roles. Mutant TDP-43 RNP granules in the mid axon also show liquid droplet formation but display slower recovery after photobleaching, indicating these liquid droplets are more viscous than TDP-43 WT granules. Increased viscosity observed in TDP-43 mutant granules may confer toxic gain of function, possibly enhancing the propensity for aggregation.

Materials and Methods

Primary Cortical Culture and Transfection. Primary cortical neurons were dissociated from embryonic day 18–20 Sprague–Dawley rat embryos at the Neuron Culture Service Center at the University of Pennsylvania, as described (52). Details are provided in *SI Materials and Methods*. Cortical neurons (days in vitro 7–10) were transfected with cDNA constructs using Lipofectamine 2000 reagent (Invitrogen).

Live-Cell Microscopy. Live imaging of cortical cultures was performed in Hibernate E (Brainbits) supplemented with 2% (vol/vol) B27 and 2 mM GlutaMAX in a temperature-controlled chamber mounted on an inverted NikonTi microscope with apochromat 63× and 100× 1.49-N.A. oil-immersion objectives; images were acquired on a PerkinElmer UltraVIEW VOX spinning disk confocal system equipped with an Ultraview Photokinesis (PerkinElmer) unit and a C9100-50 EMCCD camera (Hamamatsu) controlled by Volocity software (PerkinElmer). Axons were identified by morphological criteria (53, 54) and were imaged at one frame every 2–3 s for 5–10 min. Near-TIRF microscopy was performed as described (55). Images were captured on an ImagEM C9100-13 (Hamamatsu) camera at a rate of seven to 10 frames per second × 2 min using 50- to 90-ms exposure times. For hexanediol experiments, cortical neurons expressing EGFP–TDP-43 were treated with either 5 μg/mL digitonin alone (control) or 5 μg/mL digitonin (Sigma) with 4% (wt/vol) 1,6-hexanediol (Acros Organics) and then imaged at 5-min intervals for 25 min.

FRAP and photoactivation/photoconversion experiments were performed using the Ultraview Photokinesis module. EGFP–TDP-43 was photobleached using the 488-nm laser at 75–90% power for 30 cycles, with a 1-ms spot period within a region of interest (0.5 × 0.5 μm). Images were acquired using the 488-nm laser at one frame every second for 3–5 s before and 120–180 s subsequent to photobleaching. The photokinesis unit was calibrated before each experiment to ensure tightly localized half-bleach, as described elsewhere (1). Photoactivation/conversion of mEos3.2–TDP-43 or PAGFP-Synapsin was performed using the 405-nm laser at 2–3% power for 30 cycles, with a 2-ms spot period (41–43, 56).

STED Superresolution Microscopy. STED microscopy was performed at the University of Pennsylvania Microscopy Core on a Leica DMI 6000 Inverted laser scanning confocal microscope equipped with 592-nm and 660-nm STED

depletion lasers. Detailed immunofluorescence methods are provided in *SI Materials and Methods*.

Image and Data Analysis. All image processing and analysis were performed using ImageJ/Fiji and/or custom automated analyses in MATLAB R2015a (MathWorks). For a more clear presentation of Fig. 2, Figs. S3 and S4, and Movies S1 and S2, time series were denoised as described (57). However, all data analysis was performed on the raw, unprocessed data as described (58, 59). Full details of image, data, and statistical analysis are described in *SI Materials and Methods*.

ACKNOWLEDGMENTS. We thank Mariko Tokito, the Neuron Culture Service Center, and Margie Price for technical assistance. We thank Ekaterina Grishchuk, Amy Ghiretti, Sandra Maday, Swathi Ayloo, Andrea Stavoe, and Michael Howland for thoughtful discussion and comments on the manuscript. This research was supported by the NIH under Awards R37 NS060698 (to E.L.F.H.), 1-K08-NS094744 (to P.P.G.), and F30NS092227 (to J.J.N.).

1. Brangwynne CP, et al. (2009) Germline P granules are liquid droplets that localize by controlled dissolution/condensation. *Science* 324(5935):1729–1732.
2. Brangwynne CP, Mitchison TJ, Hyman AA (2011) Active liquid-like behavior of nucleoli determines their size and shape in Xenopus laevis oocytes. *Proc Natl Acad Sci USA* 108(11):4334–4339.
3. Kroschwald S, et al. (2015) Promiscuous interactions and protein disaggregases determine the material state of stress-inducible RNP granules. *eLife* 4:e06807.
4. Zhu L, Brangwynne CP (2015) Nuclear bodies: The emerging biophysics of nucleoplasmic phases. *Curr Opin Cell Biol* 34:23–30.
5. Hyman AA, Weber CA, Jülicher F (2014) Liquid-liquid phase separation in biology. *Annu Rev Cell Dev Biol* 30:39–58.
6. Patel A, et al. (2015) A liquid-to-solid phase transition of the ALS protein FUS accelerated by disease mutation. *Cell* 162(5):1066–1077.
7. Weber SC, Brangwynne CP (2012) Getting RNA and protein in phase. *Cell* 149(6): 1188–1191.
8. Hyman AA, Brangwynne CP (2011) Beyond stereospecificity: Liquids and mesoscale organization of cytoplasm. *Dev Cell* 21(1):14–16.
9. King OD, Gitler AD, Shorter J (2012) The tip of the iceberg: RNA-binding proteins with prion-like domains in neurodegenerative disease. *Brain Res* 1462:61–80.
10. Kwiatkowski TJ, Jr, et al. (2009) Mutations in the FUS/TLS gene on chromosome 16 cause familial amyotrophic lateral sclerosis. *Science* 323(5918):1205–1208.
11. Vance C, et al. (2009) Mutations in FUS, an RNA processing protein, cause familial amyotrophic lateral sclerosis type 6. *Science* 323(5918):1208–1211.
12. Kim HJ, et al. (2013) Mutations in prion-like domains in hnRNPA2B1 and hnRNPA1 cause multisystem proteinopathy and ALS. *Nature* 495(7442):467–473.
13. Han TW, et al. (2012) Cell-free formation of RNA granules: Bound RNAs identify features and components of cellular assemblies. *Cell* 149(4):768–779.
14. Kato M, et al. (2012) Cell-free formation of RNA granules: Low complexity sequence domains form dynamic fibers within hydrogels. *Cell* 149(4):753–767.
15. Molliex A, et al. (2015) Phase separation by low complexity domains promotes stress granule assembly and drives pathological fibrillization. *Cell* 163(1):123–133.
16. Lin Y, Protter DS, Rosen MK, Parker R (2015) Formation and maturation of phase-separated liquid droplets by RNA-binding proteins. *Mol Cell* 60(2):208–219.
17. Burke KA, Janke AM, Rhine CL, Fawzi NL (2015) Residue-by-residue view of in vitro FUS granules that bind the C-terminal domain of RNA polymerase II. *Mol Cell* 60(2):231–241.
18. Murakami T, et al. (2015) ALS/FTD mutation-induced phase transition of FUS liquid droplets and reversible hydrogels into irreversible hydrogels impairs RNP granule function. *Neuron* 88(4):678–690.
19. Holt CE, Schuman EM (2013) The central dogma decentralized: New perspectives on RNA function and local translation in neurons. *Neuron* 80(3):648–657.
20. Kiebler MA, Bassell GJ (2006) Neuronal RNA granules: Movers and makers. *Neuron* 51(6):685–690.
21. Krichevsky AM, Kosik KS (2001) Neuronal RNA granules: A link between RNA localization and stimulation-dependent translation. *Neuron* 32(4):683–696.
22. Ou SH, Wu F, Harrich D, García-Martínez LF, Gaynor RB (1995) Cloning and characterization of a novel cellular protein, TDP-43, that binds to human immunodeficiency virus type 1 TAR DNA sequence motifs. *J Virol* 69(6):3584–3596.
23. Buratti E, Baralle FE (2001) Characterization and functional implications of the RNA binding properties of nuclear factor TDP-43, a novel splicing regulator of CFTR exon 9. *J Biol Chem* 276(39):36337–36343.
24. Elvira G, et al. (2006) Characterization of an RNA granule from developing brain. *Mol Cell Proteomics* 5(4):635–651.
25. Fallini C, Bassell GJ, Rossoll W (2012) The ALS disease protein TDP-43 is actively transported in motor neuron axons and regulates axon outgrowth. *Hum Mol Genet* 21(16):3703–3718.
26. Alami NH, et al. (2014) Axonal transport of TDP-43 mRNA granules is impaired by ALS-causing mutations. *Neuron* 81(3):536–543.
27. Sreedharan J, et al. (2008) TDP-43 mutations in familial and sporadic amyotrophic lateral sclerosis. *Science* 319(5870):1668–1672.
28. Kabashi E, et al. (2008) TARDBP mutations in individuals with sporadic and familial amyotrophic lateral sclerosis. *Nat Genet* 40(5):572–574.
29. Neumann M, et al. (2006) Ubiquitinated TDP-43 in frontotemporal lobar degeneration and amyotrophic lateral sclerosis. *Science* 314(5796):130–133.
30. Johnson BS, et al. (2009) TDP-43 is intrinsically aggregation-prone, and amyotrophic lateral sclerosis-linked mutations accelerate aggregation and increase toxicity. *J Biol Chem* 284(30):20329–20339.
31. Schmidt HB, Rohatgi R (2016) In vivo formation of vacuolated multi-phase compartments lacking membranes. *Cell Reports* 16(5):1228–1236.
32. Elden AC, et al. (2010) Ataxin-2 intermediate-length polyglutamine expansions are associated with increased risk for ALS. *Nature* 466(7310):1069–1075.
33. Stone HA (1994) Dynamics of drop deformation and breakup in viscous fluids. *Annu Rev Fluid Mech* 26:65–102.
34. Kasza KE, et al. (2007) The cell as a material. *Curr Opin Cell Biol* 19(1):101–107.
35. Zajac AL, Goldman YE, Holzbaur EL, Ostap EM (2013) Local cytoskeletal and organelle interactions impact molecular-motor-driven early endosomal trafficking. *Curr Biol* 23(13):1173–1180.
36. Weiss AN, Bittner MA, Holz RW, Axelrod D (2014) Protein mobility within secretory granules. *Biophys J* 107(1):16–25.
37. Sinnecker D, Voigt P, Hellwig N, Schaefer M (2005) Reversible photobleaching of enhanced green fluorescent proteins. *Biochemistry* 44(18):7085–7094.
38. Axelrod D, Koppel DE, Schlessinger J, Elson E, Webb WW (1976) Mobility measurement by analysis of fluorescence photobleaching recovery kinetics. *Biophys J* 16(9):1055–1069.
39. Zhang H, et al. (2015) RNA controls PolyQ protein phase transitions. *Mol Cell* 60(2): 220–230.
40. Elbaum-Garfinkle S, et al. (2015) The disordered P granule protein LAF-1 drives phase separation into droplets with tunable viscosity and dynamics. *Proc Natl Acad Sci USA* 112(23):7189–7194.
41. Zhang M, et al. (2012) Rational design of true monomeric and bright photoactivatable fluorescent proteins. *Nat Methods* 9(7):727–729.
42. Lippincott-Schwartz J, Patterson GH (2009) Photoactivatable fluorescent proteins for diffraction-limited and super-resolution imaging. *Trends Cell Biol* 19(11):555–565.
43. Patterson GH, Lippincott-Schwartz J (2002) A photoactivatable GFP for selective photolabeling of proteins and cells. *Science* 297(5588):1873–1877.
44. Patel SS, Belmont BJ, Sante JM, Rexach MF (2007) Natively unfolded nucleoporins gate protein diffusion across the nuclear pore complex. *Cell* 129(1):83–96.
45. Corrado L, et al. (2009) High frequency of TARDBP gene mutations in Italian patients with amyotrophic lateral sclerosis. *Hum Mutat* 30(4):688–694.
46. Van Deerlin VM, et al. (2008) TARDBP mutations in amyotrophic lateral sclerosis with TDP-43 neuropathology: A genetic and histopathological analysis. *Lancet Neurol* 7(5): 409–416.
47. Liu-Yesucevitz L, et al. (2014) ALS-linked mutations enlarge TDP-43-enriched neuronal RNA granules in the dendritic arbor. *J Neurosci* 34(12):4167–4174.
48. Jain S, et al. (2016) ATPase-modulated stress granules contain a diverse proteome and substructure. *Cell* 164(3):487–498.
49. Ganassi M, et al. (2016) A surveillance function of the HSPB8-BAG3-HSP70 chaperone complex ensures stress granule integrity and dynamism. *Mol Cell* 63(5):796–810.
50. Polymenidou M, et al. (2011) Long pre-mRNA depletion and RNA missplicing contribute to neuronal vulnerability from loss of TDP-43. *Nat Neurosci* 14(4):459–468.
51. Puthanveettil SV (2013) RNA transport and long-term memory storage. *RNA Biol* 10(12):1765–1770.
52. Wilcox KS, Buchhalter J, Dichter MA (1994) Properties of inhibitory and excitatory synapses between hippocampal neurons in very low density cultures. *Synapse* 18(2): 128–151.
53. Craig AM, Banker G (1994) Neuronal polarity. *Annu Rev Neurosci* 17:267–310.
54. Kaech S, Banker G (2006) Culturing hippocampal neurons. *Nat Protoc* 1(5):2406–2415.
55. Tokunaga M, Imamoto N, Sakata-Sogawa K (2008) Highly inclined thin illumination enables clear single-molecule imaging in cells. *Nat Methods* 5(2):159–161.
56. Ballister ER, Ayloo S, Chenoweth DM, Lampson MA, Holzbaur EL (2015) Optogenetic control of organelle transport using a photocaged chemical inducer of dimerization. *Curr Biol* 25(10):R407–R408.
57. Kervrann C, Boulanger J (2006) Optimal spatial adaptation for patch-based image denoising. *IEEE Trans Image Process* 15(10):2866–2878.
58. Twelvetrees AE, et al. (2016) The dynamic localization of cytoplasmic dynein in neurons is driven by kinesin-1. *Neuron* 90(5):1000–1015.
59. Tarantino N, et al. (2014) TNF and IL-1 exhibit distinct ubiquitin requirements for inducing NEMO-IKK supramolecular structures. *J Cell Biol* 204(2):231–245.